PCCP

Accepted Manuscript

ROYAL SOCIETY OF CHEMISTRY

www.rsc.org/pccp

TOC

Graphene oxide sheets provides short-range electron transfer from glucose oxidase enzyme to electrode surface

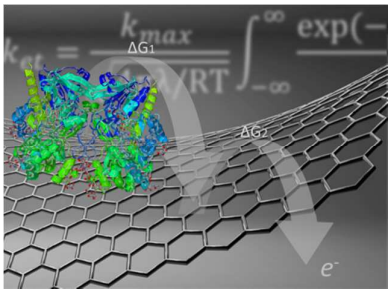

Cite this: DOI: 10.1039/c0xx00000x

www.rsc.org/xxxxxx

ARTICLE TYPE

Evidence of Short-Range Electron Transfer of a Redox Enzyme on Graphene Oxide Electrodes

Marccus V. A. Martins[a], Andressa R. Pereira[b], Roberto A. S. Luz[a], Rodrigo M. Iost[b], and Frank N. Crespilho*[b]

Received (in XXX, XXX) Xth XXXXXXXXX 20XX, Accepted Xth XXXXXXXXX 20XX
DOI: 10.1039/b000000x

Direct electron transfer (DET) between redox enzymes and electrode surfaces is of growing interest and an important strategy in the development of biofuel cells and biosensors. Among the nanomaterials utilized at electrode/enzyme interfaces to enhance electronic communication, graphene oxide (GO) has been identified as a highly promising candidate. It is postulated that GO layers decrease the distance between the flavin cofactor (FAD/$FADH_2$) of the glucose oxidase enzyme (GOx) and the electrode surface, though experimental evidence concerning the distance dependence of the rate constant of heterogeneous electron-transfer (k_{het}) has not yet been observed. In this work, we report the experimentally observed DET of the GOx enzyme adsorbed on flexible carbon fiber (FCF) electrodes modified with GO (FCF-GO), where the k_{het} between GO and electroactive GOx has been measured at a structurally well-defined interface. Curves obtained from the Marcus theory were used to obtain k_{het}, by using the model proposed by Chidsey. In agreement with experimental data, this model proved be useful to systematically probe the dependence of electron transfer rates on distance, in order to provide an empirical basis to understand the origin of interfacial DET between GO and GOx. We also demonstrate that the presence of GO at the enzyme/electrode diminishes the activation energy by decreasing the distance between the electrode surface and FAD/$FADH_2$.

Introduction

Direct electron transfer (DET) between redox enzymes and electrode surfaces is of great interest because of their potential importance in the enzyme kinetics and in the development of new generations of biosensors and biofuel cells that require rapid, well-defined electron transfer. For instance, several molecular models to explain the DET between the glucose oxidase (GOx) enzyme and electrode surfaces have been proposed.[1,2] GOx is a structurally rigid glycoprotein of 160 kDa with a hydrodynamic radius of 43 Å, consisting of two identical polypeptide chains, each containing a flavin adenine dinucleotide (FAD/$FADH_2$) center.[3,4] Following the first reports on DET with a redox active protein in 1977,[5,6] several authors have reported the DET of GOx in differing electrode configurations.[7,8] The effect of protein environments on the facilitation of DET is a fundamental problem in enzyme catalysis with implications on a wide range of materials from bioanodes in biofuel cells[9] to third generation biosensor design.[10] As the FAD redox active center of GOx is deeply buried in a glycoprotein shell, electrochemical DET from the FAD of GOx to an electrode surface is very slow. The elucidation of factors that hinder electron transfer is central to technological improvements. In the investigation of such factors, Heller and co-workers reported[1,7] that the distance dependence of the electron-transfer rate is central to understanding why some experimental conditions can lead to DET; electron transfer rates between the enzyme and electrode surface decay exponentially with the distance. It is therefore unsurprising—given the macromolecular size of enzymes—that GOx does not efficiently communicate with electrode surfaces; natural systems often need to transfer electrons with high directional specificity over distances greater than 14 Å. In order to enhance the electronic communication in such processes, one line of enquiry has been the incorporation of materials on electrodes surfaces which facilitate better electron transfer.

DET has recently been reported in which nanomaterials such as nanoparticles[11], nanotubes[12], graphene oxide (GO)[13] and reduced graphene oxide[14] (rGO) have been incorporated on electrodes. Although there is no experimental data to rationalize the occurrence of DET, it is postulated that the nanomaterials enhance the electronic communication. To this end, GO is a promising material in the promotion of DET, due to the single layers of carbon atoms that can organize themselves in a closely packed two-dimensional honeycomb lattice on the electrode surface,[15] leading to a high surface activity area and fast rates of DET. However, no evidence exists at the molecular level as to why an interface composed of GO between the electrode and GOx enzyme promotes fast DET. Few well-defined experimental systems are available to probe fundamental issues such as the dependence of interfacial electron transfer rates on the reaction free energy, the electron-transfer distance, or the molecular structure of the GOx at the interface. This can be explained because, unlike for other redox systems (e.g. cytochrome c), it is very difficult to attach the FAD cofactor of GOx to the electrode

surface without altering its tertiary structure, thus making it difficult to assess the value of the heterogeneous FAD electron transfer constants as a function of the electrode distance.

In this work, the rate constant of the electron transfer reaction between a flexible carbon fiber (FCF) electrode modified with GO (FCF-GO) and electroactive GOx enzymes has been measured at a structurally well-defined interface at different temperatures. Curves obtained from the Marcus theory[16-18] were used in order to calculate heterogeneous electron transfer constants (k_{het}), using the model proposed by Chidsey.[19] The latter model proved useful to systematically probe the dependence of electron transfer rates on distance, in order to provide an empirical basis for understanding the origin of interfacial DET. Through electrochemical studies, we demonstrate that the presence of GO at the enzyme/electrode interface decreases the activation energy by shortening the distance between the electrode surface and FAD/$FADH_2$ redox couple.

Experimental details

Graphene-Oxide Formation (in situ) on FCF Electrodes. It is well known that exfoliated graphene oxide or GO can form well-dispersed aqueous colloids.[20] Stankovich and co-workers[21] have reported that solution-based routes involve the chemical oxidation of graphite to hydrophilic graphene oxide, which can be readily exfoliated as individual GO sheets by ultrasonication in water. An alternative methodology was sought to obtain graphene-oxide directly adsorbed on FCFs (FCF-GO); we used (with modifications) the chemical route proposed by Kovtyukhova and co-workers[22] for FCF exfoliation. Carbon fibers were extracted from a carbon cloth (CCS 200). The FCFs (0.5 g) were placed in H_2SO_4/$KMnO_4$ (120 mL), which was prepared from $KMnO_4$ (464 mg) dissolved in H_2SO_4 (1M). The FCFs were kept in an ultrasound bath for 3 hours, then washed with HCl (to remove the MnO_2), and distilled water.

Fibers modified with GO were characterized by infrared (IR) spectroscopy, Raman spectroscopy, field emission scanning electron microscopy (FEG-SEM), energy dispersive X-Ray spectroscopy (EDX) and X-ray diffraction (XRD). IR analyses of the FCFs were performed by Fourier-Transform infrared spectroscopy (FTIR). The FCFs were placed directly on a ZnSe diamond during the acquisition of the spectra. The experiments were carried out in ATR/absorption mode, with a Varian C640 FT-IR spectrophotometer. Raman spectra were recorded on a Jobin Yvon T-64000 spectrometer, with laser alignment at 532.14 nm; a unique fiber was isolated using an optical microscope and placed on a glass substrate in order to focus the beam. FEG-SEM (JMS-6701F, JEOL) images were obtained in order to analyze the morphological characteristics of the fibers before and after the fiber exfoliation process. Several fibers were placed on double-sided carbon tape and subsequently placed in the sample holder.

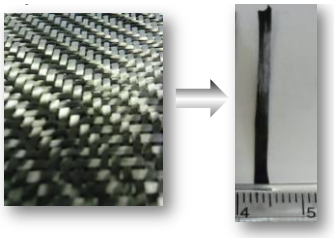

Figure 1. Carbon cloth (left) and withdrawal of a flexible carbon fiber (FCF).

FCF-GOx and FCF-GO-GOx Bioelectrodes. The FCF-GOx and FCF-GO-GOx bioelectrodes were prepared via the physical adsorption[23,24] of the enzyme. An area of the fiber (0.2 cm^2) was treated with epoxy resin. After drying the resin, the FCF was placed in the GOx solution (10 mg mL^{-1} in sodium phosphate buffer, pH 7.02) for 24 hours at 4 °C. The fiber was washed with buffer to remove non-adsorbed enzymes, and vacuum dried. Nafion solution (5%, 20 µL) was dropped onto the fiber containing the adsorbed GOx, affording the FCF-GO-GOx bioelectrode. The same procedure was performed for the untreated fiber, furnishing the FCF-GOx bioelectrode. Figure 1 shows a photograph of the carbon cloth (left) and of a fiber (right) before chemical exfoliation. The schemes in Figures S1a and b (see the Supporting Information) depict the chemical exfoliation and the enzyme immobilization processes, respectively.

FCF-GO-GOx Non-Catalytic Electrochemistry. To investigate the redox behavior and kinetic properties of the FCF-GOx and FCF-GO-GOx bioelectrodes, a conventional system of three electrodes was used: $Ag/AgCl_{sat}$ as the reference electrode, platinum as the counter electrode and the synthesized bioelectrodes as the working electrodes. All analyses were performed using a µAutolab Type III galvanostat/potentiostat apparatus.

Temperature Dependence Experiments. Electrochemical measurements to obtain the direct electron transfer of GOx were performed using a three electrode system comprising a flexible carbon fiber after chemical treatment (FCF-GO) as the working electrode, platinum as the counter electrode, and a saturated Ag/AgCl electrode as the reference electrode. Phosphate buffer solution (0.1 mol L^{-1}, pH 7.0) was used as the electrolyte, which was purged with argon for at least 30 minutes prior to the recording of voltammograms under an argon atmosphere. The temperature of the electrolyte was varied by using a thermostatic bath (GE-MultiTemp IV Thermostatic Circulator, 0.01 ºC resolution). The internal temperature of the electrochemical cell was also monitored by a thermometer. The study of the DET of GOx at different temperatures was carried out between 5.0 ºC and 37.0 ºC at pH 7.0.

Influence of pH on DET. To study the influence of pH on DET, the electrochemical measurements were performed using a three electrode system as described above. The study at varying pH was carried out between pH 5.5 and 8.0 with a phosphate buffer solution (0.1 mol L^{-1}) as the electrolyte.

Biocatalytic Properties of FCF-GO-GOx. The catalytic activity of GOx in the FCF-GO-GOx bioelectrode was tested by polarization curves and chronoamperometry experiments at

differing glucose concentrations. The glucose solution (1.0 mol L^{-1}) was prepared and stored overnight. A potential of -0.3 V was applied in the chronoamperometry experiments. All experiments were performed under anaerobic conditions; oxygen was removed from the electrolyte by bubbling N_2 gas through the solution for 15 minutes.

Numerical Modeling. To interpret the electron-transfer behavior of the bioelectrodes, the Marcus theory was applied to the interfacial electron transfer between an electrode and an adsorbed redox couple. We adopted the approach of Chidsey[19] to calculate the electrochemical rate constants as a function of potential. The Butler-Volmer model[25] was also used to calculate the kinetic parameters. All calculations in this study were performed using the Matlab® software.

Results and Discussion

Graphene Oxide-Modified FCF. Figure 2 shows high-resolution FEG-SEM images of the FCF (a and b) and FCF-GO (c, d and e) at different magnifications.

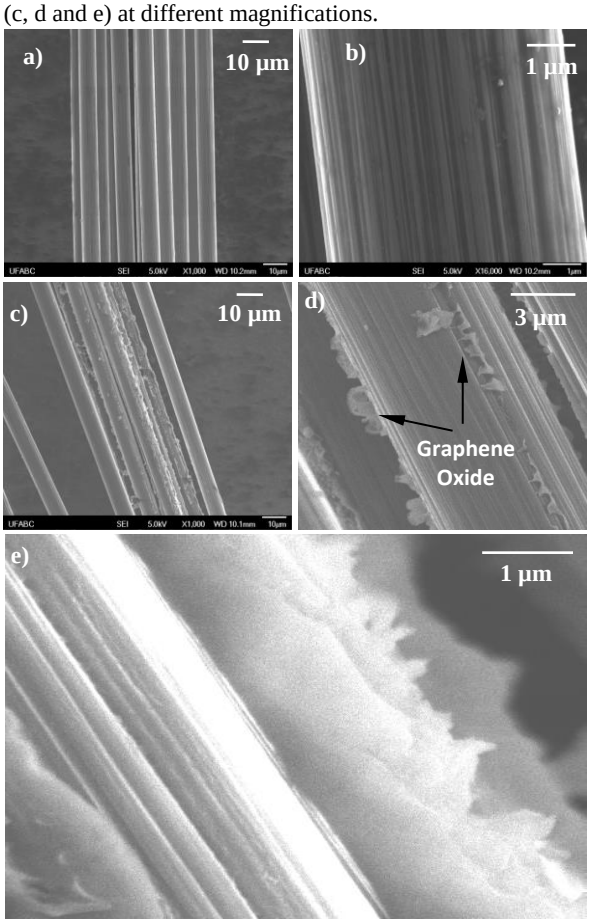

Figure 2. Field emission-scanning electron microscope (FEG-SEM) images of the FCF at different magnifications: untreated (a and b) and graphene oxide (GO)-modified fibers (FCF-GO) (c - e).

The FCF has a diameter of 6.5 µm and homogeneous morphology, characteristic of FCFs in general. Following treatment with $H_2SO_4/KMnO_4$ solution, the morphology of the fiber surfaces change considerably. In the images shown in Figure 2c-e, there are various aggregates randomly affixed that suggest graphene is adsorbed in a disorderly fashion. In comparison to other studies reported in the literature,[21,26] GO has a structure similar to that observed in the images. To confirm the presence of GO, the FCFs were characterized by Raman spectroscopy.

Figure 3a shows an optical micrograph of the green laser focalization on the FCF surface. Figure 3b shows the Raman spectra for the untreated FCF (black line) and FCF-GO (red line). Both spectra show two bands at about 1360 cm^{-1} (D band), assigned to the scattering of the graphite edges,[27] and at 1580 cm^{-1} (G band), assigned to the first order E_{2g} mode[28] of the C-C bond. Graphite materials usually exhibit two Raman bands in the active spectrum near 1575 and 1355 cm^{-1}.[29] However, small shifts in this region and changes in the band intensities indicate changes in bond lengths and angles.[30] The maximum intensity D (ID) and G (IG) bands for the FCF are exactly identical (black line). However, it is observed that the intensity of the FCF-GO D and G bands (red line) are different. The increase in the G band is caused by the presence of graphene oxide.[30] This increase could also be attributed to a greater number of defects in the hexagonal carbon structure that constitutes the GO, as proposed by Ramesha and co-workers.[31]

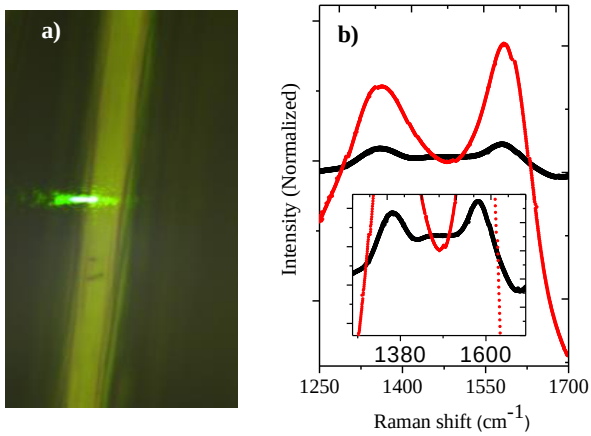

Figure 3. a) Optical microscopy images showing the focusing of a green laser (532 nm) onto the surface of a FCF using one MicroRaman. b) Raman spectrum of the FCF (black line) and FCF-GO (red line). Inset: Magnified spectrum showing the lower intensity Raman scattering of FCFs compared to FCFs treated with acid solution.

Table 1 lists values presented in the literature[26,32,33] reported for the D and G bands in GO. According to the literature, the smaller value of the ratio of D and G bands (I_D/I_G), the greater number of defects in the hexagonal carbon structure. This indicates the formation of graphene oxide within the sheets, as can be seen in the FEG-SEM images in Figure 2.

Table 1. Values of D and G bands and I_D/I_G ratio to GO

D	*G*	I_D/I_G	*Ref.*
1363	1594	0.85	20
1350	1610	0.83	26
1350	1581	0.85	27
1360	1580	0.86	*this work*

Infrared spectroscopy was performed to confirm the presence of oxygenated groups in the structure of the GO. Figure 4a shows the spectra for the untreated FCF (black line) and the FCF-GO (red line). In the spectrum of the FCF, there are two bands at 2849 and 2919 cm^{-1}, assigned to symmetrical stretching vibration modes of the C-H and C-C bonds, respectively. Also in this spectrum, there are several bands between 1700 and 1500 cm^{-1}, which can be attributed to the angular deformation modes of CH_3 and CH_2 groups. However, significant spectroscopic differences can be seen for the FCF-GO spectrum (red line). This spectrum shows a band at 3396 cm^{-1}, attributed to the stretching vibration mode of carboxylic acid O-H bonds. The bands at 2849 and 2919 cm^{-1} are assigned to the symmetrical stretch vibration modes of the C-H and C-C bonds respectively. The bands at 1643, 1386 and 1025 cm^{-1} are assigned to C=O bond stretching, O-H bond deformation, and C-O bond stretching of carboxylic acids, respectively.[34-36]

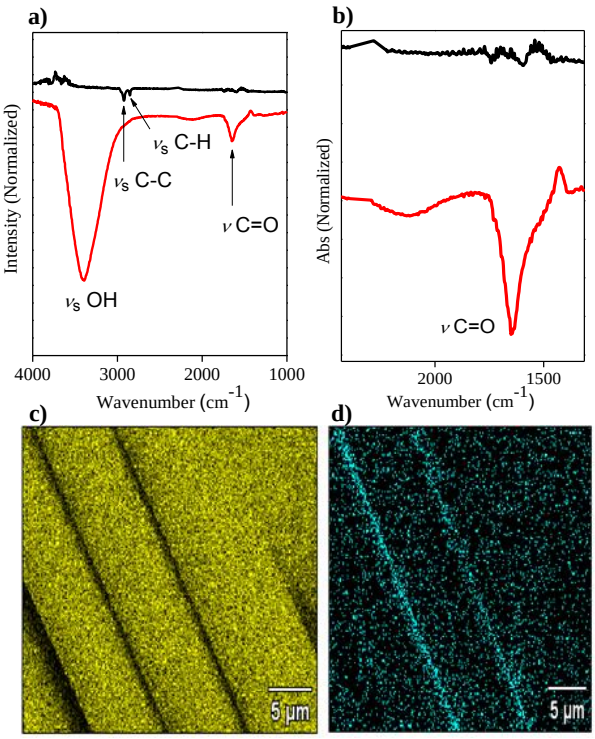

Figure 4. a) Fourier transform infrared (FTIR) spectrum of the untreated FCF (black line) and FCF-GO (red line) electrodes. b) Magnified view of FTIR spectrum of a) showing the appearance of C=O stretching bands characteristic of carboxylic acid functional groups. c) Energy dispersive X-ray spectroscopy (EDX) image showing the chemical mapping of the FCF-GO with trace elemental carbon in yellow color and d) with trace elemental oxygen in blue color.

It is known that the chemical structure of GO varies between reports, depending on the synthetic procedure.[32] There are several possible models proposed in the literature[33] based on experimental data (e.g. NMR, XRD, IR, and X-ray photoelectron spectroscopy (XPS)) to assign the chemical composition of the GO. In this instance, the spectroscopic behavior of the FCF-GO indicates that the GO is functionalized with carboxyl groups,[33] as can be seen in Figure 4b, in which the stretching mode of C=O appears with a higher intensity in the FCF-GO. Thus, the Raman and IR spectra suggest a GO structure as proposed in Figure 4c. Corroborating the previous results, the presence of hydrophilic groups in the GO structure causes changes in X-ray diffraction (XRD). Figure S3 (Supporting Information) shows the diffractograms of the FCF (black line) and the FCF-GO (red line). Both spectra show two well defined peaks, one at 2θ = 11.7° corresponding to the (001) reflection, and another at around 2θ = 25.0° corresponding to the (002) reflection.[37] The intensity of the (001) peak of the FCF-GO is greater when compared to the intensity of the FCF. Another finding is the shift of the (002) peak from 24.1° to 25.1°, as can be seen in the inset of Figure S3. In addition, the broader (002) peak is usually correlated to an interlayer spacing between the GO sheets,[38] probably due to agglomerates seen in the FEG-SEM images and the presence of –COOH groups.[39] The Raman, IR and XRD spectra are consistent with the chemical mapping images realized by EDX, in which there is the presence of elemental carbon (Figure 4c) and oxygen (Figure 4d).[40] It is also possible that epoxide and alcohol groups are present, as suggested in the model proposed by Dreyer and co-workers.[41]

Direct Electron Transfer of GOx on FCF-GO. Before investigating the redox properties of the GOx immobilized on the fibers, the electrochemical behaviors of the carbon fibers before and after the formation of GO were evaluated. Figure 5a shows cyclic voltammograms for both the FCF (black line) and the FCF-GO (blue line) in the potential region between 0.0 and -0.8 V vs. Ag/AgCl. Both the FCF and FCF-GO electrodes exhibit similar electrochemical behavior in sodium phosphate buffer solution at pH 7.0, where there are no Faradaic processes. Only a small increase in the capacitive currents for the FCF-GO electrode is observed. This increase in capacitive current can be attributed to an increase in roughness of the fiber's surface, due to the presence of GO, as seen in the FEG-SEM images (Figure 2). After GOx immobilization on the FCF (or FCF-GOx) surface, two redox processes are observed, as seen in the voltammogram in Figure 5b (black line). However, when GOx is immobilized on FCF-GO (FCF-GO-GOx), a similar redox process appears both sharper and shifted to more negative potential (blue line, Figure 5b). The formal potential (E°) for both the FCF-GOx and FCF-GO-GOx bioelectrodes can be calculated from Equation 1.

$$E^0 = \frac{E_{pa}+E_{pc}}{2} \quad (1)$$

where E_{pa} and E_{pc} are the peak potentials for the anodic and cathodic process, respectively.

Applying Equation 1 obtained -0.43 V for the FCF-GOx electrode, and 0.55 V for the FCF-GO-GOx electrode. Both values are very close to the theoretical formal potential ($E^{o'}$) of the FAD of GOx vs. Ag/AgCl at pH 7.0.[37-39] The value of the potential separation between the anodic and cathodic peaks (ΔE)

were 60 and 50 mV for FCF-GOx and FCF-GO-GOx, respectively. Values below 60 mV may indicate a reversible process and a fast charge exchange[42] for the reduction/oxidation of the FAD/$FADH_2$ cofactor, as described in Equation 2.

$$FAD + 2e^- + 2H^+ \leftrightarrows FADH_2 \quad (2)$$

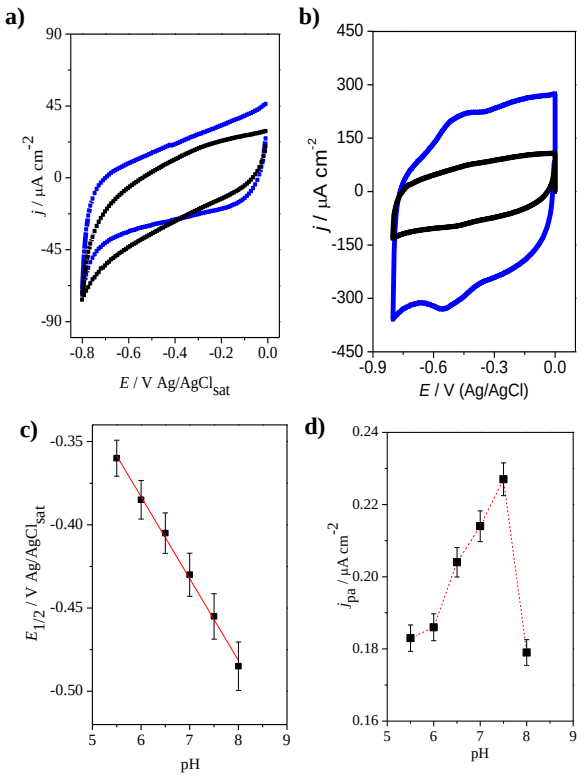

Figure 5. Cyclic voltammograms of a) FCF (black line) and FCF-GO (blue line). Scan rate: 30 mV s^{-1}. b) Cyclic voltammograms of FCF-GOx (black line) and FCF-GO-GOx (blue line). Scan rate: 100 mV s^{-1}. Electrolyte support: sodium phosphate buffer, pH 7.0. c) Plot of dependence of half-wave potential as a function of pH. d) Plot of dependence of the current density of the oxidation peak as a function of pH.

Furthermore, the bioelectrodes are very stable; anodic and cathodic peak currents do not change over 20 consecutive voltammetric cycles (see Figure S4 in Supporting Information). The pH dependence of the steady currents of the GOx oxidation/reduction was determined by monitoring experiments over the entire range from pH 5.5 to 8.0. In all pH ranges, a reversible process was observed, with the same modulus values for the oxidation and reduction currents. The difference between the peak potentials corresponded to 0.0592/*n*, where *n* is the number of electrons involved in the semi-reaction. Thus, the average value obtained from the difference between the peaks potential was 0.023±0.008, close to the theoretical reversible two-electron reaction (0.0295). The slope of the graph $E_{1/2}$ vs. pH (Figure 5c) was -49 mV/pH, close to the theoretical value (-59 mV/pH) for reversible processes in the reaction of two protons with two electrons. From the graphs in Figure 5d, it was concluded that the optimum pH for DET is between 7.0 and 7.5.

At pH 5.5 and 6.0, the redox process appears subtle enough to offset less negative potentials (see Figure S5 in Supporting Information). As the pH increases to 6.5, the process begins to appear more defined, although it is still shifted. For pH values of 7.0 and 7.5, the redox process is more clearly defined and the peak currents obtained are larger. At pH 8.0, the currents obtained are lower and the peak does not appear well-defined as compared to previous pH values. Thus, for the further experiments, the sodium phosphate electrolyte was maintained at pH 7.0

DET Temperature Dependence. The temperature dependence of the electron transfer was investigated by varying the temperature of the electrolyte from 278 to 310 K (see Figure S6 in Supporting Information). In this experiment, it is important to consider that the thermal denaturation of GOx causes dissociation of the flavin cofactor. The properties of the thermally denatured protein indicate that thermally denatured GOx adopts a compact structure, a form of molten globule-like apoenzyme.[43] The FCF-GO-GOx electrode was used in the experiments and cyclic voltammograms were recorded at 50 mV s^{-1} at five temperatures (278, 283, 298, 308 and 310 K). There was no significant change in voltammetric profile when the temperature was changed from 278 K to 283 K, though changes were more pronounced when the temperature was raised to higher values (298 K), with a smaller increase at 310 K. The increase in temperature promotes an increase in both anodic and cathodic peak currents with shift of potentials to more negative values. Figure 6a shows the decrease in E_{pa} (black dots) and E_{pc} (red dots) with increasing temperature and Figure 6b shows the increase in current density peaks j_{pa} (black dots) and j_{pc} (red dots), both in the temperature range described previously.

The experiments were repeated three times using three different electrodes, and the variability of the data was measured by considering the standard deviation and errors calculated from t-tests with a 95% confidence interval. A straight line was observed (least-squares correlation coefficient = 0.967 for the oxidation process and 0.969 for the reduction process). The presence of two redox processes is clear, as demonstrated by E_{Ox} = -0.40V and E_{Red} = -0.43V, as expected for DET of the FAD cofactor of the GOx enzyme.[7,8] The activation energy for the GOx enzyme was calculated using the Lumry-Eyring model.[44,45] Although the model assumes a transition state from a normal enzyme state to a denatured state, the temperature dependence of the electron transfer kinetics (k^0) was investigated away from the denaturation temperature of GOx in order to obtain more accurate information about DET in the same temperature range.

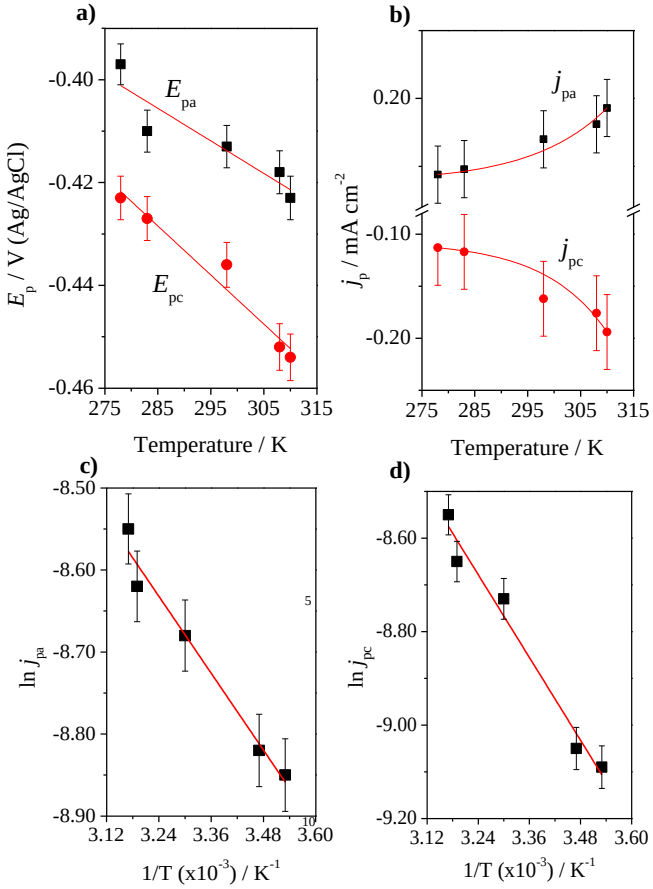

Figure 6. Plots of E_p a) and j_p b) of FCF-GO-GOx as a function of the temperature (K). Scan rate: 50 mV s^{-1}. Electrolyte: sodium phosphate buffer 7.02. Plots of ln j_{pa} c) and ln j_{pc} d) of immobilized GOx as a function of the reciprocal of temperature for E_a calculation. The experiments were obtained in triplicate using three different electrodes, and the variability of the data was measured by considering the standard deviation and errors calculated from t-tests with a 95% confidence interval. The means were plotted with error bars.

The relation of the rate constant (k_0) of the electron transfer can be described according to Equation 3.[46]

$$i_{max} = nFAk_0[E] \quad (3)$$

where n is the number of transferred electrons, F is the Faradaic constant, A is the surface area of the working electrode, and [E] is the concentration of immobilized GOx in the equilibrium. In this case, n, F, A, and [E] are constant since all experiments were obtained with the same working FCF-GO-GOx electrode. Thus, i_{max}, is directly proportional to k_0, allowing i_{max} (and consequently the current density, j_{max}) to be used in the Arrhenius plot. Some interesting studies have reported the relationship between E_a, the transfer coefficient (α), and the hidden heat of electrode process (q).[25] For instance, we use the simplest concept of Arrhenius ($k_0 = A\exp(-E_a/RT)$), where E_a is the activation energy, A is the pre-exponential factor, R is the molar gas constant (8.314 kJ mol^{-1} K^{-1}), T is the temperature in K, and k_0 the heterogeneous charge transfer reaction[16-18] in order to estimate the energy of activation (E_a) for GOx. Figures 6c and d show the plot of ln j_{pa} and ln j_{pc}, respectively, vs. the reciprocal of temperature (1/T). The apparent E_a value was obtained as 280 kJ mol^{-1} with an apparent transition temperature of 55.8±1.2°C (328.95 K).[47] The values of E_a calculated from the linear range of ln j_{max} vs. 1/T for anodic and cathodic peaks were 6.49 kJ mol^{-1} and 12.26 kJ mol^{-1}, respectively.

The standard potential E^0 is an important value as it is related to the standard free energy of the reaction $\Delta G^0_{T,p}$ and to the equilibrium constant K according to Equation (4):[48]

$$-nFE^0 = \Delta G^0_{T,p} = -RT\ln K \quad (4)$$

We can therefore use the relationship above to calculate the standard free energy of the direct electron transfer of GOx. It is known that the number of electrons n in the redox process is two, F is the Faraday constant, and E^0 is -0.55 V; ΔG^0 for the DET of GOx is therefore -106.1 kJ mol^{-1}. Table 2 shows the kinetic and thermodynamic parameters for the FCF-GO-GOx electrode configuration.

Table 2. Kinetic and thermodynamic parameters of FCF-GO-GOx.

E_0	- 0.550 V
ΔE	0.023 ± 0.008
E_a	6.49 kJ mol^{-1} (oxidation process) 12.26 kJ mol^{-1} (reduction process)
ΔG^0	- 106.1 kJ mol^{-1}

Bioelectrocatalytic Properties. To confirm that the process of enzymatic immobilization did not damage the catalytic performance of GOx toward the oxidation of glucose, biocatalytic tests were performed.

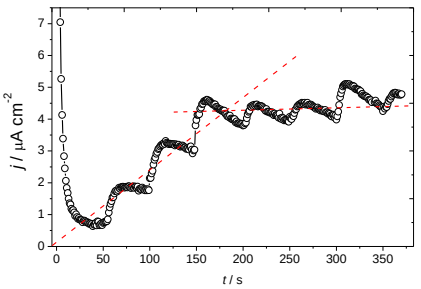

Figure 7. Chronoamperometry of the FCF-GO-GOx bioelectrode in the presence of successive additions of glucose (total glucose concentration 1 mmol L^{-1}, 2 mmol L^{-1}, 3 mmol L^{-1}, 4 mmol L^{-1}, 5 mmol L^{-1}, 6 mmol L^{-1}, and 7 mmol L^{-1}, respectively) at -0.3 V of applied potential.

Figure 7 shows a chronoamperometry experiment at -0.3 V of applied potential for 400 s. This potential was chosen because it is the value at which the current reaches a quasi-steady state for the oxidation of glucose. Accordingly, figure 7 shows the chronoamperometric response of FCF-GO-GOx in the presence of successive additions of glucose. Each addition corresponds to

an addition of 100 mL glucose at a concentration of 0.5 mol L^{-1}. The time required to achieve the quasi-steady state current shortly after the addition is 6 seconds, indicating a rapid response.[49-51] The increase in glucose concentration rapidly promotes oxidation in the chain, reaching saturation level at high concentrations, as expected by Michaelis-Menten behavior (see Figure S7 in Supporting Information). Such behavior indicates that glucose is easily oxidized at low concentrations by the FCF-GO-GOx bioelectrode and implies that FAD is active within the protein structure of GOx.

Using Marcus Theory for DET. To investigate the direct electron transfer at the electrode/enzyme interface, several voltammetric cycles at different scan rates for both the FCF-GOx and FCF-GO-GOx systems were carried out, as shown in Figures 8a and b. Increasing the scan rate promotes increased current densities of the anodic and cathodic peaks. Thus, constructing graphs of the current density dependence as a function of scan rate (υ) obtains two straight lines (Figures 8c and d). This behavior indicates two phenomena: first, that the electrochemical processes are governed by charge transfer at the GOx/FCF interface, and secondly, that the enzyme is strongly adsorbed on the carbon electrode surface. The study of heterogeneous electron transfer rates for FCF-GOx and FCF-GO-GOx bioelectrodes was explored by varying the scan rate from 10 to 2000 mV s^{-1} (see Figures S8a and b in Supporting Information). It is clearly observed that the FAD redox processes remain sharp up to 2000 mV s^{-1} for the FCF-GO-GOx bioelectrode. The linear relationship between the scan rate and the current density of the anodic and cathodic peaks also remains for both the bioelectrodes (see Figures S8c and d in Supporting Information). In Figures 8e and f, the plotted lines represent calculated rate constants for different models of electron-transfer (ET) kinetics. The dash-dot curves in Figures 8e and f are the plots of the rate constants, as predicted by the Butler-Volmer (BV) formalism:[25]

$$k_{red}^{BV} = k^0 \exp(-\alpha F(E - E^0)/RT) \quad (5)$$

$$k_{oxi}^{BV} = k^0 \exp((1 - \alpha) F(E - E^0)/RT) \quad (6)$$

where k^0 is the rate constant at zero overpotential and α is the electron transfer coefficient, which represents the degree of symmetry between the reduction and oxidation rate constants (α = ½ for the symmetrical case). By using Laviron's method[25] (which is based on the BV theory), α can be determined from the slope of the straight lines of anodic (k_a) and cathodic (k_c) peak potentials versus log(υ) (Figures 8e and f) according to $\log(k_a/k_c) = \log[\alpha/(1-\alpha)]$ or also from $\log \upsilon_a/\upsilon_c = \log[\alpha/(1-\alpha)]$ and k^0 can be calculated by Equation 7:

$$k^0 = \frac{\alpha n F \upsilon_c}{RT} = \frac{(1-\alpha) n F \upsilon_a}{RT} \quad (9)$$

The α and k^0 values were estimated at 0.56 and 9.08 s^{-1} for FCF-GOx and 0.57 and 15.04 s^{-1} for FCF-GO-GOx, respectively. Although the Butler-Volmer formalism is more empirical and more commonly used than is the Marcus theory,[16-18] in this model, the activation energies for both the cathodic and anodic rate are assumed to be a linear function of overpotential and it is not considered the influence of the reorganization energy. Consequently, the classical BV equation does not represent accurate rate constant values.

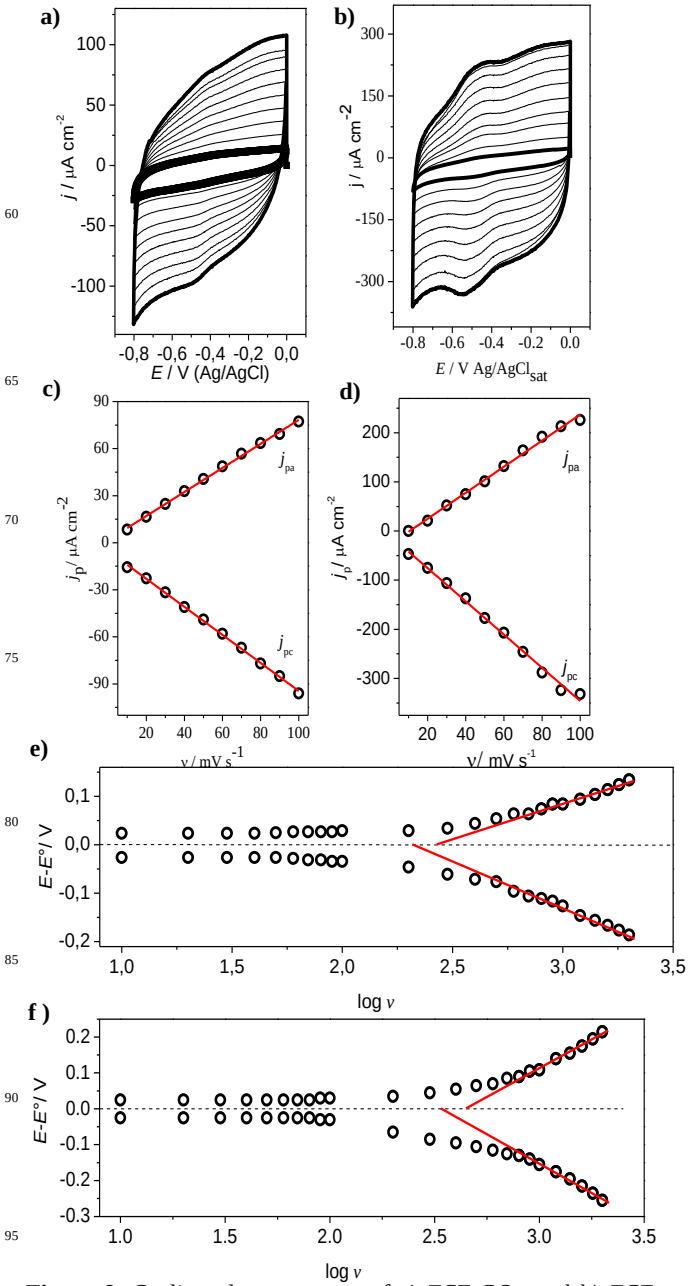

Figure 8. Cyclic voltammograms of a) FCF-GOx and b) FCF-GO-GOx at different scan rates: 10, 20, 30, 40, 50, 60, 70, 80, 90 and 100 mV s^{-1}. c) and d) the dependence of (j_{pa}) and cathodic (j_{pc}) peaks as a function of scan rate. Electrolyte support: sodium phosphate buffer, pH 7.0. Plots of variation of anodic and cathodic peak overpotential (E-E^0) as function of log υ for electrode configuration e) FFC-GO-GOx and f) FCF-GO-GOx.

The Marcus theory describes the homogeneous electron transfer between two chemical species as function of the nuclear configuration of initial and final species[16-18] using Gibbs energy diagrams.[48] The nuclear configuration is represented by two identical parabolas, as shown in Figure 9a.

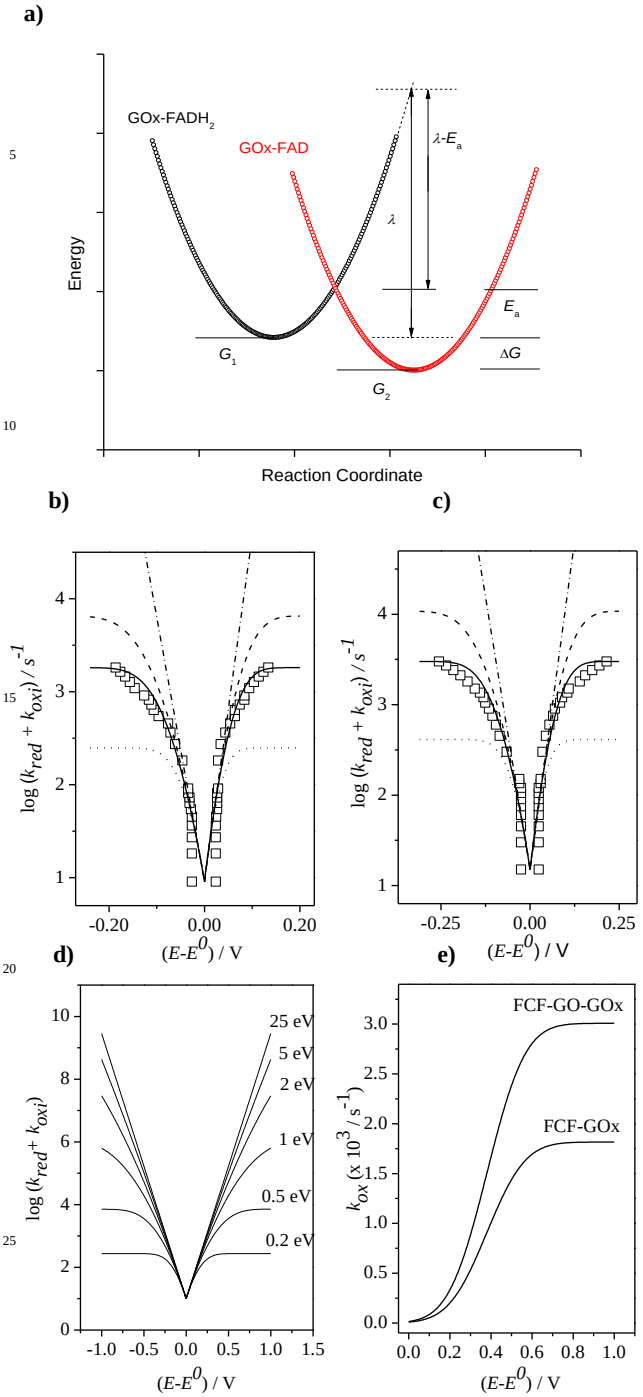

Figure 9. a) Marcus energy diagrams showing the initial (GOx-$FADH_2$) and final state (GOx-FAD) for electron transfer (ET). Plot of the measured decay rate constants (squares) at 25 ºC and calculated rate constants from Equation 8 with: λ = 0.2 eV (dots), λ = 0.38 eV (solid) and λ = 0.5 eV (dashed), and from Equation 5 and 6 (dash-dot) with k^0 = 9.08 s^{-1}, α = 0.56 for FCF-GOx and k^0 = 15.04 s^{-1}, α = 0.57 for b) FCF-GOx and c) FCF-GO-GOx. d) Plot of the measured decay rate constants (square) at 25 ºC from 25 eV to 0.2 eV. e) Oxidative ET rate constant (k_{ox}) as a function of overpotential for FCF-GOx (k^0 = 9.08 s^{-1}, α = 0.56) and FCF-GO-GOx (k^0 = 15.04 s^{-1}, α = 0.57) according to Marcus theory of interfacial ET (Equation 8 with λ = 0.38 eV).

The initial state GOx-$FADH_2$ (black dots) and final state GOx-FAD (red dots) are represented by two identical parabolas with the respective initial (G_1) and final (G_2) Gibbs energies. The intercept point between the two parabolas and the minimum energy state G_1 is represented by E_a, with the difference between the two minimum energy states (G_1 and G_2) represented by ΔG^0. In this manner, this study adopted the approach of Chidsey[19] to calculate electrochemical rate constants as a function of potential. For electron transfer between an electrode and an adsorbed redox couple, Chidsey[19] derived a relation between ET rate constants ($k_{red/oxi}$) and overpotential (E-E^0) by integrating the Marcus equation (Equation 8), which describes the ET rate using the Fermi-Dirac distribution, since electron transfer can occur to or from any Fermi level in the electrode:

$$k_{red/oxi} = \frac{k_{max}}{\sqrt{4\pi\lambda/RT}} \int_{-\infty}^{\infty} \frac{\exp(-1/4\lambda RT[\lambda \pm F(E-E^0)-RTx]^2)}{1+\exp(x)} dx \quad (8)$$

where λ is the reorganization energy in eV (the energy required to reorient all atoms from the equilibrium state to the product state). k_{max} is the maximum electron-transfer rate constant at high overpotential, and is given by Equation 9:

$$k_{max} = \frac{4\pi^2 V_0^2}{N_A h RT} \exp(-\beta r) \quad (9)$$

where V_0 represents the degree of electronic coupling, r is the distance between donor and acceptor (in Å) and β is the decay coefficient (in $Å^{-1}$). Rate constants can be numerically evaluated from Equation 6 using the method described by Heering and co-workers.[52] This method was used to calculate the plots of k_{red} + k_{oxi} against E-E^0 in Figures 9b and c for different values of reorganization energy (lines). The curve with λ = 0.38 eV was the best fit; this λ value was used to generate the curves for FCF-GOx and FCF-GO-GOx plotted in Figures 9b and c. As predicted by the Marcus theory[16-18], at a low driving force, the rate increases exponentially (Figure 9d) and then asymptotically approaches a maximum plateau value (k_{max}) at a sufficiently large overpotential, from which the rate constants become independent of the driving force, passing through k_{max}/2 when the overpotential equates λ (Figure 9e).[53-55] The maximum rate constant achieved for FCF-GO-GOx was approximately twice that for FCF-GOx. Such an increase corresponds to the presence of graphene structures, which facilitate the charge exchange mechanism.

Short-Range Electron Transfer on FCF-GO. Some studies[1,7] have reported the dependence of the electron-transfer rate constant on the distance (d) between the redox center and the electrode surface. According to Equation 10, derived from the Marcus theory[16-18], $k_{red/ox}$ decreases linearly with increasing distance (as shown in Figure 10).

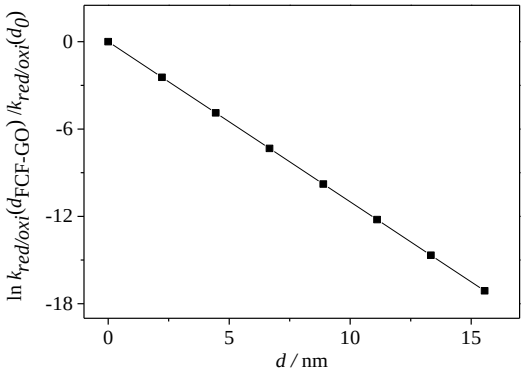

Figure 10. Dependence of ln $k_{red/oxi}(d_{FCF-GO})/k_{red/oxi}(d_0)$ as a function of distance (d).

Equation 8 can be rewritten for GOx modified by FCF-GO and FCF bioelectrodes according to Equations 11 and 12, respectively, where d_{FCF-GO} and d_{FCF} are the distances between the redox center and the FCF surfaces with and without graphene oxide. d_0 is related to a redox center on the electrode surface (i.e., zero distance).

$$k_{red/oxi}(at\ d_2) = k_{red/oxi}(at\ d_1)\exp\left[-\beta(d_2 - d_1)\right] \quad (10)$$

$$k_{red/oxi}(\text{at}\ d_{FCF-GO}) = k_{red/oxi}(at\ d_0)\exp\left[-\beta(d_{FCF-GO})\right] \quad (11)$$

$$k_{red/oxi}(\text{at}\ d_{FCF}) = k_{red/oxi}(at\ d_0)\exp\left[-\beta(d_{FCF})\right] \quad (12)$$

The electron tunneling constant (β) has been determined for a number of different redox-active self-assembled systems,[56-58] and these measurements show that the tunneling constant is somewhat insensitive to the identity of a redox center for the group spacer. In this way, assuming the same β for both bioelectrodes, the ratio of d_{FCF-GO} and d_{FCF} is given by Equation 13:

$$ln\left[\frac{k_{red/oxi}(\text{at}\ d_{FCF-GO})}{k_{red/oxi}(\text{at}\ d_{FCF})}\right] = \frac{d_{FCF-GO}}{d_{FCF}} \quad (13)$$

Substituting the electron transfer rate constants calculated from Equation 6 for FCF-GO-GOx and FCF-GOx into Equation 11, it is observed that the presence of graphene oxide decreases by half the distance between GOx redox center and FCF surface ($d_{FCF-GO} = 0.5\ d_{FCF}$).

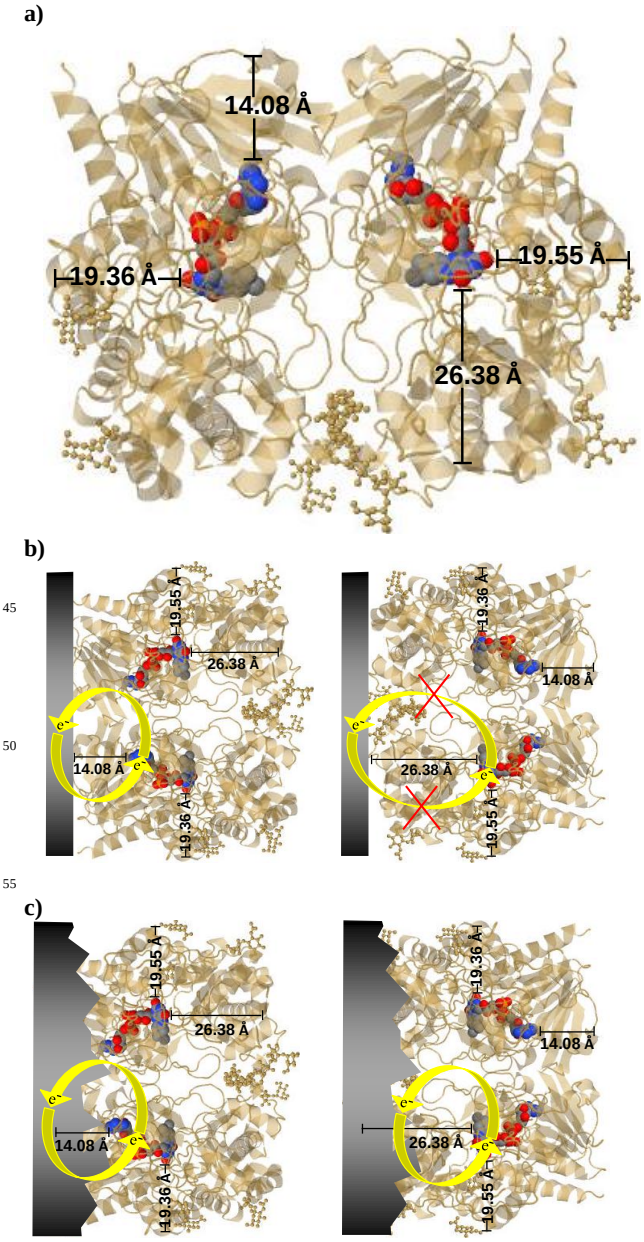

Figure 11. a) Position of the flavin adenine dinucleotide (FAD) within the GOx enzyme dimer. The positions were obtained from the JPD database (Jmol Version 12.2.15). The colored balls represent the FAD. (b) Example of two situations for adsorption on dimeric GOx. On the left, a dimeric-GOx molecule with SER-244 is close to the electrode surface (at the bottom). The minimum distance (d) between the flavin and the surface of the monomer is about 13 Å. On the top, glycosaminoglycans regions of dimeric-GOx are adsorbed on the electrode, with d >13 Å. The two isoalloxazine moieties are separated by a large distance of about 40 Å. On the right, the same structure was simulated in the same conditions and directions in space, where the protein chain was omitted for better visualization of the FAD cofactor. Data simulation with point group: Cyclic–C2; stoichiometry: Homo 2-mer-A2. Resolution structures can found in reference 59.

Thus, regarding to the results obtained yet, further details should be considered. It is worth mentioned that in this study, the low redox current observed in voltammograms of GOx immobilized directly on FCF without treatment is attributed to the absence of GO. For redox enzymes and other biological molecules, the minimal distance between redox centers and the electrode can be expressed as the distance separating the electron donor and acceptor species. The consensus among previous reports is that in order to favor efficient electron tunneling, the distance between them should be 14 Å or less,[1,7] the latter also including the photosynthetic center. In this way, the in situ-exfoliated GO decreases the distance between the FAD and the FCF, as represented in Figure 11a. According to the JPD simulation, the FAD is not situated in the center of the enzyme. Generally (including this work) the adsorption method for enzyme immobilization does not guide the enzymes to a specific orientation. Thus, the enzyme may adsorb randomly on the surface of the FCF. Consequently, the longest distances between the FAD and the periphery of the enzyme shell are 19.36, 19.55, and 26.38 Å. As the SEM-FEG images of the FCF without treatment showed a homogeneous morphology, one possible explanation for the low redox current of FCF-GOx bioelectrodes is the adsorption of the enzyme on the FCF through the position with minimum distance (e.g. 14.08 Å), as showed in Figure 11b. Conversely, the presence of GO directly exfoliated from the surface of FCF facilitates the electron change when the enzyme is adsorbed via the positions with greater distances (e.g. 19.36, 19.55 and 26.38 Å), as can be seen simulated in Figure 11c. The presence of GO allows the FAD exchanging electrons through of all simulated distance, increasing the redox current. The behavior of GO in promoting DET is well reported in the literature,[60-63] due to properties such as extraordinary electron transfer[64,65] and high special surface area.[66] In contrast to these studies, which produce modified electrodes with graphene structures through two or more steps, as a result of this study we have produced a FCF electrode modified with GO to promote the DET of GOx in a single step.

Conclusions

In this paper, we report the DET of GOx on reliably synthesized FCF electrodes modified with GO, where the k_{het} between GO and electroactive GOx has been measured at a structurally well-defined interface. Curves obtained via the approach of Chidsey[19] were used to calculate the electrochemical rate constants as a function of potential. Chidsey[19] derived the relation between ET rate constants and overpotential by integrating the Marcus equation, which describes the ET rate using the Fermi-Dirac distribution. The curve with $\lambda = 0.38$ eV was the experimentally determined value, which was used to generate the curves for FCF-GOx and FCF-GO-GOx plotted in Figure 9. In agreement with experimental data, this model proved be useful to systematically probe the dependence of electron transfer rates on distance, in order to provide an empirical basis to understand the origin of interfacial DET between GO and GOx. The maximum rate constant achieved for FCF-GO-GOx was approximately twice that of FCF-GOx. Such an increase corresponds to the presence of GO structures, which facilitate the charge exchange mechanism. Substituting the electron transfer rate constants into Equation 11, it is observed that the presence of GO decreases the distance between GOx redox center and FCF surface by half ($d_{FCF\text{-}GO} = 0.5\ d_{FCF}$). Thus, the model presented in Figure 11 is plausible, where the presence of GO facilitates the electron change when the enzyme is adsorbed via the position with greater distances. We believe that the most important result in this study is the experimental and theoretical evidence that the presence of GO at interface enzyme/electrode diminishes the activation energy by decreasing the distance between the electrode surface and enzyme cofactor.

Acknowledgements

The authors gratefully acknowledge financial support from FAPESP (F.N. Crespilho, Project numbers: 2011/01541-0 and 2013/04663-4), CNPq (Project numbers: 304255/2010-6 and 478525/2013-3), INEO, and Rede NanoBioMed-Brasil (CAPES).

Notes and references

[a] *Centro de Ciências Naturais e Humanas, Universidade Federal do ABC, 09210-170, Santo André, SP, Brazil*
[b] *Instituto de Química de São Carlos, Universidade de São Paulo, 13560-970, São Carlos, SP, Brazil*
**frankcrespilho@iqsc.usp.br*

† Electronic Supplementary Information (ESI) available: Details of the synthesis of GO, immobilization of GOx, XRD of FCF and FCF-GO and cyclic voltammetry. See DOI: 10.1039/b000000x/

1 Degani, Y.; Heller, A. *J. Am. Chem. Soc.*, 1988, **110**, 2615-2620.
2 Liu, Y.; Wang, M.; Zhao, F.; Xu, Z.; Dong, S. *Biosens. Bioelectron.* 2005, **21**, 984-988.
3 Wilson, R.; Turner, A. P. F. *Biosens. Bioelectron.*, 1992, **7**, 165-185.
4 Bankar, S. B.; Bule, M. V.; Singhal, R. S.; Ananthanarayan, L. *Biotechnol. Adv.*, 2009, **27**, 489-501.
5 Kuznetsov, B. A.; Mestechkina, N. M.; Shumakovich, G. P. *Bioelectrochem. Bioenerg.*, 1977, **4**, 1-17.
6 Degani, Y.; Heller, A. *J. Am. Chem. Soc.*, 1989, **111**, 2357-2358.
7 Degani, Y.; Heller, A. *J. Phys. Chem.*, 1987, **91**, 1285-1289.
8 Liang, W.; Zhuobin, Y. *Sensors*, 2003, **3**, 544-554.
9 Davis, F.; Higson, S. P. J. *Biosens. Bioelectron.*, 2007, **22**, 1224-1235.
10 Wang, J. *Chem. Rev.*, 2008, **108**, 814-825.
11 Zhao, S.; Zhang, K.; Bai, Y.; Yang, W.; Sun, C. *Bioelectrochemistry*, 2006, **69**, 158-163.
12 Guiseppi-Elie, A.; Lei, C. H.; Baughman, R. H. *Nanotechnology*, 2002, **13**, 559-564.
13 Shan, C.; Yang, H.; Song, J.; Han, D.; Ivaska, A.; Niu, L. *Anal. Chem.*, 2009, **81**, 2378-2382.
14 Luo, Z.; Yuwen, L.; Han, Y.; Tian, J.; Zhu, X.; Weng, L.; Wang, L. *Biosens. Bioelectron.*, 2012, **36**, 179-185.
15 Pumera, M. *Chem. Soc. Rev.*, 2010, **39**, 4146-4157.
16 Marcus, R. A. *J. Chem. Phys.*, 1956, **24**, 966-978.
17 Marcus, R. A. *Annu. Rev. Phys. Chem.*, 1964, **15**, 155-196.
18 Marcus, R. A.; Sutin, N. *Biochim. Et Biophys. Acta*, 1985, **811**, 265-322.
19 Chidsey, C. E. D. *Science*, 1991, **251**, 919-922.
20 Stankovich, S.; Piner, R. D.; Nguyen, S. T.; Ruoff, R. S. *Carbon*, 2006, **44**, 3342-3347.
21 Stankovich, S.; Dikin, D. A.; Piner, R. D.; Kohlhaas, K. A.; Kleinhammes, A.; Jia, Y.; Wu, Y.; Nguyen, S. T.; Ruoff, R. S. *Carbon* 2007, **45**, 1558-1565.
22 Kovtyukhova, N. I.; Ollivier, P. J.; Martin, B. R.; Mallouk, T. E.; Chizhik, S. A.; Buzaneva, E. V.; Gorchinskiy, A. D. *Chem. Mater.*, 1999, **11**, 771-778.
23 Sassolas, A.; Blum, L. J.; Leca-Bouvier, B. D. *Biotechnol. Adv.*, 2012, **30**, 489-511.
24 Iost, R. M.; Crespilho, F. N. *Biosens. Bioelectron.*, 2012, **31**, 1-10.

25 Laviron, E. *J. Electroanal. Chem*., 1979, **100**, 263-270.
26 Stoller, M. D.; Park, S.; Zhu, Y.; An, J.; Ruoff, R. S. *Nano Lett.*, 2008, **8**, 3498-3502.
27 Fu, C.; Yang, W.; Chen, X.; Evans, D. G. *Electrochem. Commun.*, 2009, **11**, 997-1000.
28 Tai, F. C.; Wei, C.; Chang, S. H.; Chen, W. S. J. *Raman Spectrosc.*, 2010, **41**, 933-937.
29 Ni, Z.; Wang, Y.; Yu, T.; Shen, Z. *Nano Research*, 2008, **1**, 273-291.
30 Ferrari, A. C. *Solid State Commun*., 2007, **143**, 47-57.
31 Ramesha, G. K.; Sampath, S. *J. Phys. Chem. C*, 2009, **113**, 7985-7989.
32 Gao, W.; Alemany, L. B.; Ci, L.; Ajayan, P. M. *Nature Chem.*, 2009, **1**, 403-408.
33 Pumera, M. *Chem. Soc. Rev.*, 2010, **39**, 4146-4157.
34 Hontorialucas, C.; Lopezpeinado, A. J.; Lopezgonzalez, J. D. D.; Rojascervantes, M. L.; Martinaranda, R. M. *Carbon*, 1995, **33**, 1585-1592.
35 Szabo, T.; Berkesi, O.; Dekany, I. *Carbon*, 2005, **43**, 3186-3189.
36 Titelman, G. I.; Gelman, V.; Bron, S.; Khalfin, R. L.; Cohen, Y.; Bianco-Peled, H. *Carbon*, 2005, **43**, 641-649.
37 Salimi, A.; Sharifi, E.; Noorbakhsh, A.; Soltanian, S. *Biosens. Bioelectron*., 2007, **22**, 3146-3153.
38 Xiao, Y.; Patolsky, F.; Katz, E.; Hainfeld, J. F.; Willner, I. *Science*, 2003, **299**, 1877-1881.
39 Zhang, Y.; Shen, Y.; Han, D.; Wang, Z.; Song, J.; Li, F.; Niu, L. *Biosens. Bioelectron.*, 2007, **23**, 438-443.
40 Yang, S.; Feng, X.; Wang, L.; Tang, K.; Maier, J.; Müllen, K. *Angew. Chem. Int. Ed.*, 2010, **49**, 4795-4799
41 Dreyer, D. R,; Park, S.; Bielawski, C. W.; Ruoff, R. S. *Chem. Soc. Rev.*, 2010, **39**, 228-240.
42 Bard, A. J.; Faulkner, L. R. *Electrochemical Methods: Fundamentals and Applications*, 2nd ed.; John Wiley & Sons: New York, 2001.
43 Swoboda, B. E. P.; Massey, V. *J. Biol. Chem.*, 1965, **240**, 2209-2215.
44 Lumry, R.; Eyring, H. *J. Phys. Chem.*, 1954, **58**, 110-120.
45 Sanchez-Ruiz, J. M. *Biophys. J.*, 1954, **61**, 921-935.
46 Luo, W. J.; Zhu, C. F.; Su, S.; Li, D.; He, Y.; Huang, Q.; Fan, C. H. *ACS Nano*, 2010, **4**, 7451-7458.
47 Zoldák, G.; Zubrik, A.; Musatov, A.; Stupák, M.; Sedlák, E. *J. Biol. Chem.*, 2004, **279**, 47601-47609.
48 Scholz, F. *Electroanalytical Methods: Guide to Experiments and Applications*, 2nd edition.; New York: Springer, 2010.
49 You, J.-M.; Jeon, S. *Electroanalysis*, 2011, **23**, 2103-2108.
50 Wang, B. Q.; Li, B.; Deng, Q.; Dong, S. *J. Anal. Chem.*, 1998, **70**, 3170-3174.
51 Jia, W.-Z.; Wang, K.; Zhu, Z.-J.; Song, H.-T.; Xia, X.-H. *Langmuir*, 2007, **23**, 11896-11900.
52 Heering, H. A.; Hirst, J.; Armstrong, F. A. *J. Phys. Chem. B*, 1998, **102**, 6889-6902.
53 Tender, L.; Carter, M. T.; Murray, R. W. *Anal. Chem.*, 1994, **66**, 3173-3181.
54 Eckermann, A. L.; Feld, D. J.; Shaw, J. A.; Meade, T. J. *Coord. Chem. Rev*., 2010, **254**, 1769-1802.
55 Weber, K.; Creager, S. E. *Anal. Chem.*, 1994, **66**, 3164-3172.
56 Miller,C.; Cuendet, P.; Gratzel, M. *J. Phys. Chem.*, 1991, **95**, 877-886.
57 Finklea, H, O.; Hanshew. D. D. *J. Am. Chem. Soc*., 1992, **114**, 3173-3181.
58 Hong, H-G.; Park, W. *Langmuir*, 2001, **17**, 2485-2492.
59 Wohlfahrt, G. S.; Witt, J.; Hendle, D.; Schomburg, H.; Kalisz, M.; Hecht, H. *J. Acta Crystallogr*., 1999, **55**, 969-977.
60 Shan, C.; Yang, H.; Song, J.; Han, D.; Ivaska, A.; Niu, L. *Anal. Chem.*, 2009, **81**, 2378-2382.
61 Kang, X.; Wang, J.; Wu, H.; Aksay, I. A.; Liu, J.; Lin, Y. *Biosens. Bioelectron*., 2009, **25**, 901-905.
62 Shao, Y.; Wang, J.; Wu, H.; Liu, J.; Aksay, I. A.; Lin, Y. *Electroanalysis*, 2010, **22**, 1027-1036.
63 Wu, P.; Shao, Q.; Hu, Y.; Jin, J.; Yin, Y.; Zhang, H.; Cai, C. *Electrochim. Acta*, 2010, **55**, 8606-8614.
64 Li, X.; Zhang, G.; Bai, X.; Sun, X.; Wang, X.; Wang, E.; Dai, H. *Nat. Nanotechnol.*, 2008, **3**, 538-542.
65 Zhang, Y. B.; Tan, Y. W.; Stormer, H. L.; Kim, P. *Nature*, 2005, **438**, 201-204.
66 Li, D.; Mueller, M. B.; Gilje, S.; Kaner, R. B.; Wallace, G. G. *Nat. Nanotechnol.*, 2008, **3**, 101-105.